23 Nov 2001

Inferring Liquid Chaotic Dynamics in Bubble Columns

M. Cassanello

F. Larachi

A. Kemoun

M. (Muthanna) H. Al-Dahhan
Missouri University of Science and Technology, aldahhanm@mst.edu

et. al. For a complete list of authors, see https://scholarsmine.mst.edu/che_bioeng_facwork/1353

Recommended Citation

M. Cassanello et al., "Inferring Liquid Chaotic Dynamics in Bubble Columns," *Chemical Engineering Science*, vol. 56, no. 21 thru 22, pp. 6125 - 6134, Elsevier, Nov 2001.
The definitive version is available at https://doi.org/10.1016/S0009-2509(01)00218-4

PERGAMON

Chemical Engineering Science 56 (2001) 6125–6134

Chemical Engineering Science

www.elsevier.com/locate/ces

Inferring liquid chaotic dynamics in bubble columns using CARPT

M. Cassanello[a,*], F. Larachi[b], A. Kemoun[c], M. H. Al-Dahhan[c], M. P. Dudukovic[c]

[a] *PINMATE, Departmento de Industrias, FCEyN, Universidad de Buenos Aires, Ciudad Universitaria, 1428 Buenos Aires, Argentina*
[b] *Department of Chemical Engineering, Université Laval, Ste-Foy, Québec, Canada G1K 7P4*
[c] *Chemical Reaction Engineering Laboratory (CREL), Washington University, One Brookings Drive, St. Louis, MO 63130, USA*

Abstract

Experiments carried out to study the liquid displacements in bubble columns via the computer automated radioactive particle tracking technique are analyzed by means of Lagrangian and qualitative dynamics tools. The Lagrangian approach yields the detailed motion sequences of the tracer as entrained by the fast ascending bubbles or by the liquid flow alongside the column walls. The qualitative dynamics tools, on the other hand, provide prima facie corroboration of chaos in liquid motion based on an analysis of the volume-averaged Kolmogorov entropy and the mutual information function. Other features of the chaotic motion, the reconstructed attractors and the radial and axial distributions of Lyapunov exponents, are noted. Variations in the liquid hydrodynamics due to changes in column diameter and operating pressure are inspected. By increasing pressure the attractor's correlation dimension and the information loss rate decrease, whereas the liquid flow path is dramatically affected. © 2001 Published by Elsevier Science Ltd.

Keywords: Bubble columns; CARPT; Bubble wakes; Chaotic dynamics; Kolmogorov entropy; Gas–liquid flow

1. Introduction

Owing to their simple construction and low operating costs, bubble columns are among the most ubiquitous gas–liquid contactors in industry. They are widely used in such diverse fields as petrochemical, chemical, biochemical, and pharmaceutical industries and water pollution abatement. Despite tremendous research investment in studies of bubble columns, their design and scale-up are a difficult task which, by and large, still relies on semi-empirical relations (Deckwer & Schumpe, 1993). This state of affairs stems mainly from the complex bubble-induced hydrodynamics. For instance, it is only in the past few years that the chaotic nature of the bubbling phenomenon has been recognized (Tritton & Egdell, 1993; Mittoni, Schwarz, & La Nauze, 1995; Tufaile & Sartorelli, 2000). Ever since, the "hydrodynamic" chaos in bubble columns has been inferred from the analysis of pressure fluctuation time series (Letzel, Schouten, Krishna, & van den Bleek, 1997; Ranade & Utikar, 1999; Kang, Cho, Woo, Kim, & Kim, 2000).

Over the past few years, several advanced "time-resolved" techniques for non-invasively probing multiphase flows such as in bubble columns have become available (Chaouki, Larachi, & Dudukovic, 1997). Computer-automated radioactive particle tracking (CARPT), which provides non-invasively the actual trajectory of a tracing element with the same density of the liquid, is a suitable method for in-depth observations into the complex liquid dynamics in 3-D opaque and large bubble columns. Hence, conveniently prepared "flow-followers" provide local and instantaneous information from every region of the vessel under study if the time observation window is wide enough. In the last decade, many contributions have been reported providing information extracted from experiments carried out by CARPT (see for example Degaleesan, 1997; Chen et al., 1999 and references therein).

The present study analyzes, from a different approach, some of the experiments collected by CARPT in an attempt to gain further insights into the fundamentals of liquid dynamics in bubble columns. More precisely, the

* Corresponding author. Tel.: +54-11-4576-3383; fax: +54-11-4576-3366.
E-mail address: miryan@di.fcen.uba.ar (M. Cassanello).

0009-2509/01/$ - see front matter
PII: S0009-2509(01)00218-4

Table 1
Experimental conditions

Column diameter (m)	0.10	0.16	0.16 (0.3 MPa)	0.19	0.44
Static liquid height (m)	1.36	0.98	1.50	1.15	1.79
Dynamic liquid height (m)	1.60	1.20	1.90	1.37	2.10
Distributor features open area (%)	0.23	0.62	0.05	0.10	0.08
Hole size $\times 10^3$ (m)	0.5	1	0.4	0.33	0.76
Overall gas holdup (%)	15.0	18.6	21.0	16.0	14.7

trajectories of a radioactive tracer conveying information on the liquid motion within vessels of four different diameters at pressures of 0.1 and 0.3 MPa, are examined and discussed using Lagrangian (LT) and qualitative dynamics tools (QDT). The features of the tracer actual paths, revealed by LT, are observed in detail and correlated with the motion of large bubbles. On the other hand, QDT helped in diagnosing the liquid chaotic dynamics by examining features of the underlying attractors. Volume-averaged and local quantifiers of the liquid dynamics information loss rate are also estimated.

2. Experimental

The batchwise liquid dynamics experiments were performed using compressed air and tap water. Four cylindrical Plexiglas columns of internal diameters 0.10, 0.16, 0.19 and 0.44 m, operated within the ranges $0.04 \leqslant U_G \leqslant 0.05$ m/s and $0.1 \leqslant P \leqslant 0.3$ MPa and equipped with perforated plates, were studied. The heterogeneous flow regime was observed in the columns at atmospheric pressure and the homogeneous flow regime at high pressure condition.

Table 1 lists the vessel size, bed static and dynamic heights, distributors' features and overall gas holdup. For the sake of good statistics and depending on column size, the data for each CARPT experiment were acquired at 50 Hz over 18–36 h non-stop periods of time using simultaneously 16–26 $2'' \times 2''$ NaI(Tl) scintillation detectors. Further details on CARPT hardware, the system's calibration, and the rendition software are available in Degaleesan (1997).

The tracer was made by embedding an inert ^{45}Sc cylinder into a 2.4-mm polypropylene sphere. Through neutron bombardment, ^{45}Sc was turned into radioactive ^{46}Sc emitting, ca. – 1 MeV hard γ-rays impinging on the scintillation detectors' network. A tiny air hole was allowed in the polypropylene matrix so as to prepare a tracer with a density of 1050 kg/m^3 (Degaleesan, 1997). For the high pressure experiment, which pertains to a set of preliminary essays, a thin thread had to be glued to the tracer to ensure that it visits the whole column. This was checked by the axial distribution of the tracer positions in the column.

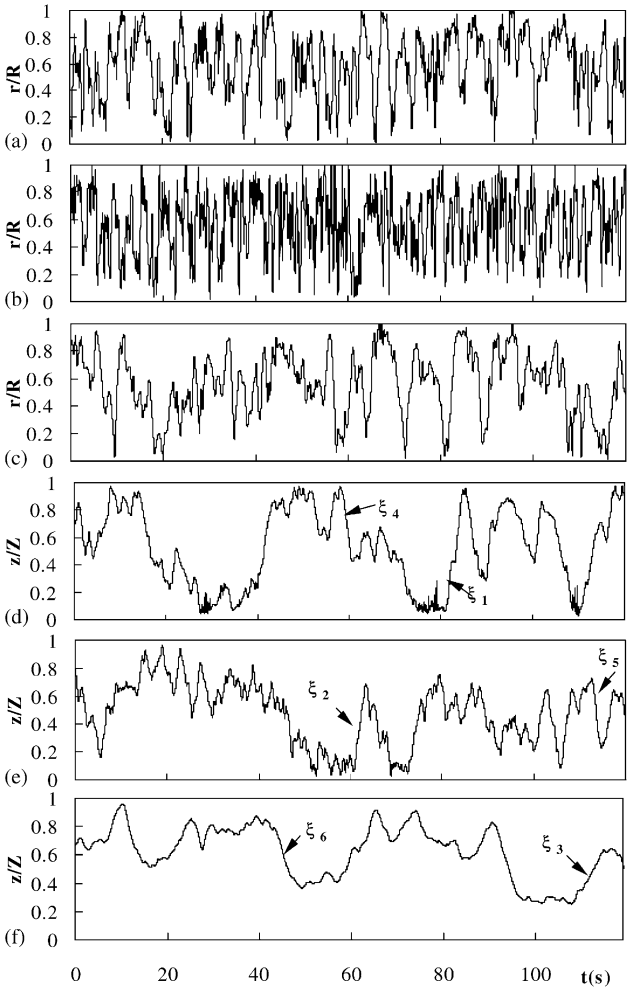

Fig. 1. Representative 2 min periods of the tracer radial and axial coordinates' time series at $U_G = 0.05$ m/s (a, d) $D_c = 0.44$ m, $P = 0.1$ MPa (b, e) $D_c = 0.16$ m, $P = 0.1$ MPa (c, f) $D_c = 0.16$ m, $P = 0.3$ MPa. ξ_1–ξ_6 are a few persistent and fast rising and descending portions in these periods.

3. Results and discussion

3.1. Trajectory analysis using Lagrangian tools

Representative 2-min histories of the tracer paths are depicted in Figs. 1a–f for the radial and axial directions to illustrate the impact of column diameter and pressure

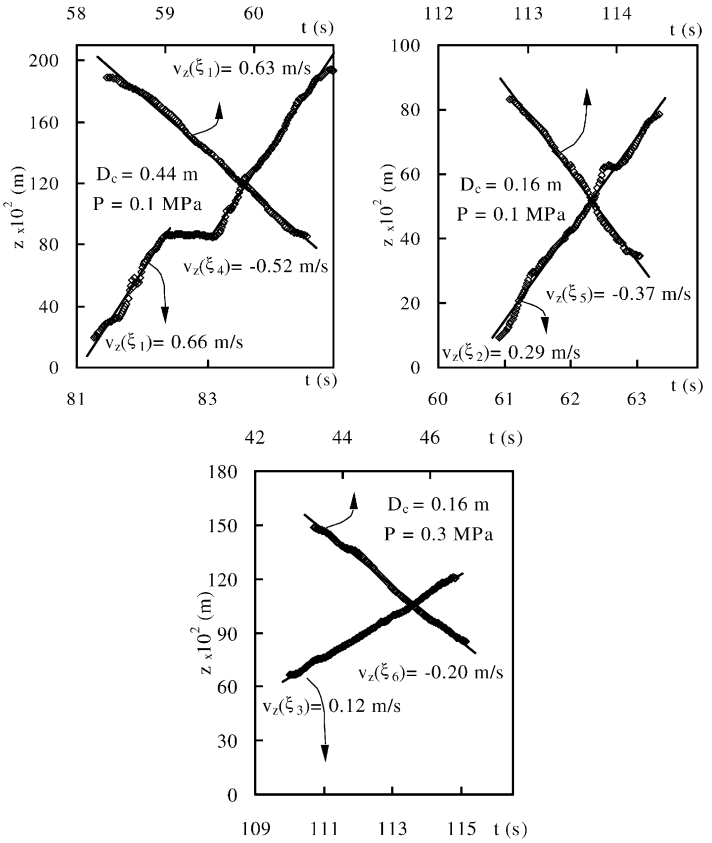

Fig. 2. Zoom of the fast rising and descending journeys in tracer movements ξ_i shown in Fig. 1 together with best line fit and corresponding velocities (slopes).

change. Similar patterns are observed for the tracer motion during the whole CARPT experiments. The confining influence of vessel walls on the tracer radial motion is apparent (Figs. 1a and b). Wall hindrance occasions a more jittery radial motion in smaller diameter vessels (Fig. 1b). As a result of shifting the regime from the churn turbulent to the dispersed bubbly flow, a three-fold increase in pressure markedly reduces the liquid radial motion fluctuations (see Figs. 1b and c).

Examination of the corresponding axial motion reveals that the less pronounced wall effect in bringing back and forth the liquid in the larger column allows more persistent vertical displacements, exhibiting steep dz/dt slopes in ascending and descending journeys (Figs. 1d and e). Consequently, such journeys may extend uninterruptedly from the distributor to the freeboard (Fig. 1d). By increasing pressure, everything else being the same, the liquid axial motion becomes smoother. Virtually, fast ascending journeys almost disappear and the tracer may remain at a given height for a few seconds, wandering between the wall and the vessel centerline (Figs. 1c and f). As argued by Larachi, Cassanello, Chaouki, and Guy (1996) for CARPT in a three-phase fluidized bed, the most likely explanation for the fast ascending rises is by entrapment of the tracer within the wake region of ascending bubbles. Then, it is possible to infer some information on the behavior of the "wake-generating" bubbles within a multi-bubble system, as the one found in a bubble column, by simply studying these ascending vertical displacements.

Fig. 2 zooms out the fast rising and descending journeys shown as ξ_1–ξ_3, ξ_4–ξ_6 in Fig. 1. The enlargement reveals that there is an interaction region in the rising path ξ_1. During the ξ_1–ξ_6 journeys, the tracer moves at an almost constant axial velocity, obtained as the best linear fit to z vs. t. Hence, a probability distribution of the liquid velocity while entrapped in a wake can be calculated. The limits and modes of the thus calculated distributions are given in Table 2. For comparison, large and small bubble rise velocities (u_{lb}, u_{sb}) estimated using the Wilkinson, Spek, and van Dierendonck (1992) approach are also shown. In the larger-diameter column the liquid velocity distribution is very skewed forwards, with values even larger than 1 m/s. The most probable liquid velocity (mode) is quite larger than in the 0.16 m diameter column and compares well with the Wilkinson et al. (1992) prediction for large bubbles velocity. For the smaller column, the mode of the velocity distribution of the bubble-wake-entrapped-liquid is closer to the predicted velocity for small bubbles "u_{sb}" (Table 2) and the distribution is more symmetric. At 0.3 MPa, the velocity distribution of liquid fast rising journeys is narrower than

Table 2
Features of the tracer fast rising journeys found during the 24 h track and properties of the bubble-wake influence domain inferred from them. $U_G = 0.05$ m/s

Column diameter (m)	0.44	0.16	0.16 (0.3 MPa)
Limits and modes of liquid fast	$0.12 \leqslant v_z \leqslant 1.37$	$0.09 \leqslant v_z \leqslant 0.62$	$0.11 \leqslant v_z \leqslant 0.48$
rising velocity distribution (m/s)	0.41	0.24	0.21
u_{lb}, u_{sb} (m/s)[a]	0.26; 0.43	0.26; 0.43	0.25; 0.38
Minor axis $a \times 10^2$ (m)	$0.3 \leqslant a \leqslant 14.6$	$0.1 \leqslant a \leqslant 9.4$	$0.6 \leqslant a \leqslant 9.8$
Major axis $b \times 10^2$ (m)	$2 \leqslant b \leqslant 42$	$0.6 \leqslant b \leqslant 12.3$	$0.8 \leqslant b \leqslant 13.6$
Distance from ellipse centroid to column centerline $d \times 10^2$ (m)	$1 \leqslant d \leqslant 21$	$0.2 \leqslant d \leqslant 7.4$	$0.4 \leqslant d \leqslant 7.4$
Area of the most probable ellipse $\times 10^4$ (m^2)	143	45	28
(% Cross-sectional area)	9%	25%	16%

[a]Calculated according to Wilkinson et al. (1992).

at atmospheric pressure, with a mode value also close to the predicted u_{sb} for this condition (Table 2).

Further analysis of ξ_1–ξ_3, ξ_4–ξ_6 portions is shown in Fig. 3 in the (r,z) and (x,y) planes. An arrow highlights where a path starts. For the rising journeys, the projected area in the (x,y) plane of the bubble-wake influence domain is approximated by ellipses (Figs. 3c, e and f). The rising journey (ξ_1) is decomposed as two paths, before and after the interaction region, so that two ellipses are drawn to enclose the wake domains. Before interaction, ξ_1 exhibits weak radial zigzag motion (Fig. 3a). After interaction the radial zigzag intensifies, especially near the freeboard where the leading bubble likely sheds the wake off. Journeys ξ_2 and ξ_3 are spiral-like and consistent with the spiral/rocking rising movements of coalesced bubbles or bubble clusters, as recently observed using optical visualization techniques (Chen, Reese, & Fan, 1994; Brucker, 1999). This behavior is particularly clear in the 0.16 m column diameter (ξ_2 in Fig. 3b), where fast bubbles appear close to the vessel centerline (Figs. 3e and f). On the contrary, the fast bubbles are not necessarily confined to the centerline region in the larger diameter column and may travel across the whole vessel cross section (Fig. 3c).

The fast descending journeys occur mostly in the $r/R > 0.5$ region (Figs. 3g and h). They are preferentially initiated close to the freeboard in the larger column. At elevated pressure, another frequent region occurs around $z/Z = 0.2$–0.3 and corresponds to a strong circulatory liquid motion that takes place close to the distributor.

Probability distributions of the parameters describing the bubble-wake domain containing ellipses are shown in Figs. 4a–d for the larger diameter column. For details on how these parameters are defined and calculated, the reader is referred to Larachi et al. (1996). The parameters' variation intervals are listed in Table 2. The minor- (a) and major-axis (b) distributions are rather skewed (Figs. 4a and b). The ratio $b/a \gg 1$, found in most cases, implies that the zigzag motion tends to be 2-D. The distance between the ellipse centroid and the column centerline is almost symmetrically distributed around a value equal to $R/2$ (Fig. 4c). The ellipses are always eccentric with respect to the column centerline ($d > 0.05R$). Their orientation is evaluated by means of the angle between the ellipse major axis and the column x-axis. The angle distribution is flat (Fig. 4d), suggesting that the spiraling is equiprobable circumferentially. Similar distributions have been found for $D_c = 0.16$ m except that the ratio b/a is considerably smaller, indicating that 3-D spiraling/rocking motions are promoted in small-diameter columns. High pressure generated skewness in a, b and d distributions.

Using the modes of the a and b distributions, the areas of the most probable ellipses delineating the wake region of influence are calculated and listed in Table 2. These areas are up to 3 times larger in the larger column at 0.1 MPa. They diminish with increasing pressure. Both observations are determined by the attainable bubble sizes. Though in absolute terms the estimated wake-region-of-influence area is larger for the 0.44 m diameter column, the corresponding percentage of cross-sectional area is relatively small (Table 2).

By assuming that each vertex in the saw-toothed z vs. t chart (Figs. 1d–f) corresponds to detachment of the tracer from the bubble wake (Larachi et al., 1996), an axial profile of the wake-liquid exchange intensity can be evaluated. These axial profiles for the runs at 0.1 MPa are shown in Figs. 4e and f for the large and small columns, respectively. The exchange intensity peaks in the freeboard for the large column, where bubbles may grow significantly.

3.2. Trajectory analysis using qualitative dynamics tools

3.2.1. Reconstructed attractors and correlation dimension

The qualitative dynamics of a system may be inferred from a time series of a characteristic variable. By considering delayed vectors of this time series, the attractor that fully describes the time evolution of the system can be reconstructed in an embedding space (Takens, 1981; Hilborn, 1994).

The motion of the tracer used in CARPT is an outcome of the different forces acting upon it. Therefore,

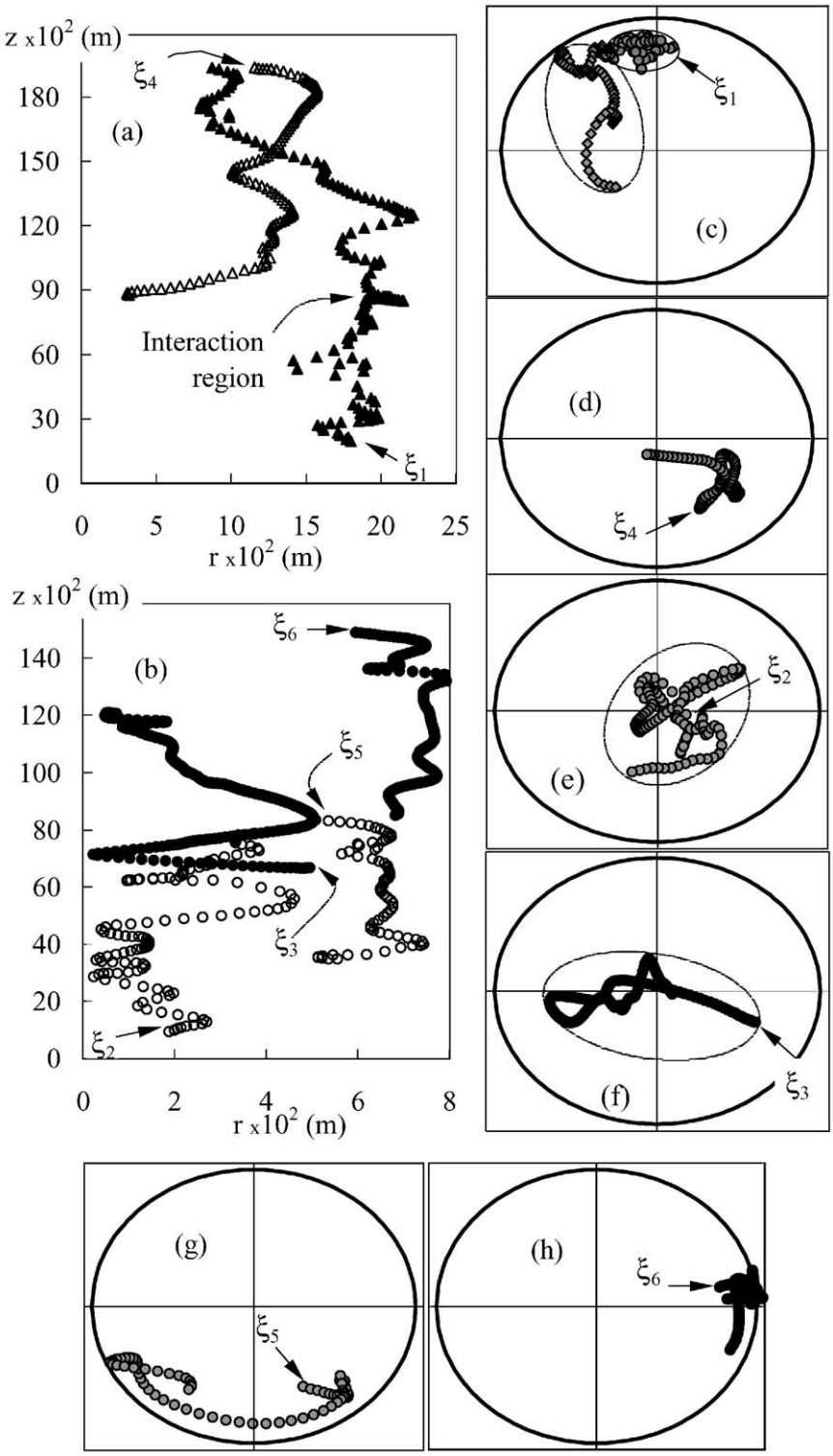

Fig. 3. Some r–z and x–y projections of the tracer fast displacements ξ_i of Fig. 1.

in this case, it conveys thorough information on the liquid dynamics in bubble columns. The time series of any of the tracer coordinates enables reconstruction of the attractors in an embedding space. Attractor reconstruction using raw noisy unfiltered experimental data leads generally to a fuzzy image. The Singular Value Decomposition procedure (Broomhead & King, 1986) enables the extraction of the most dominant components of the

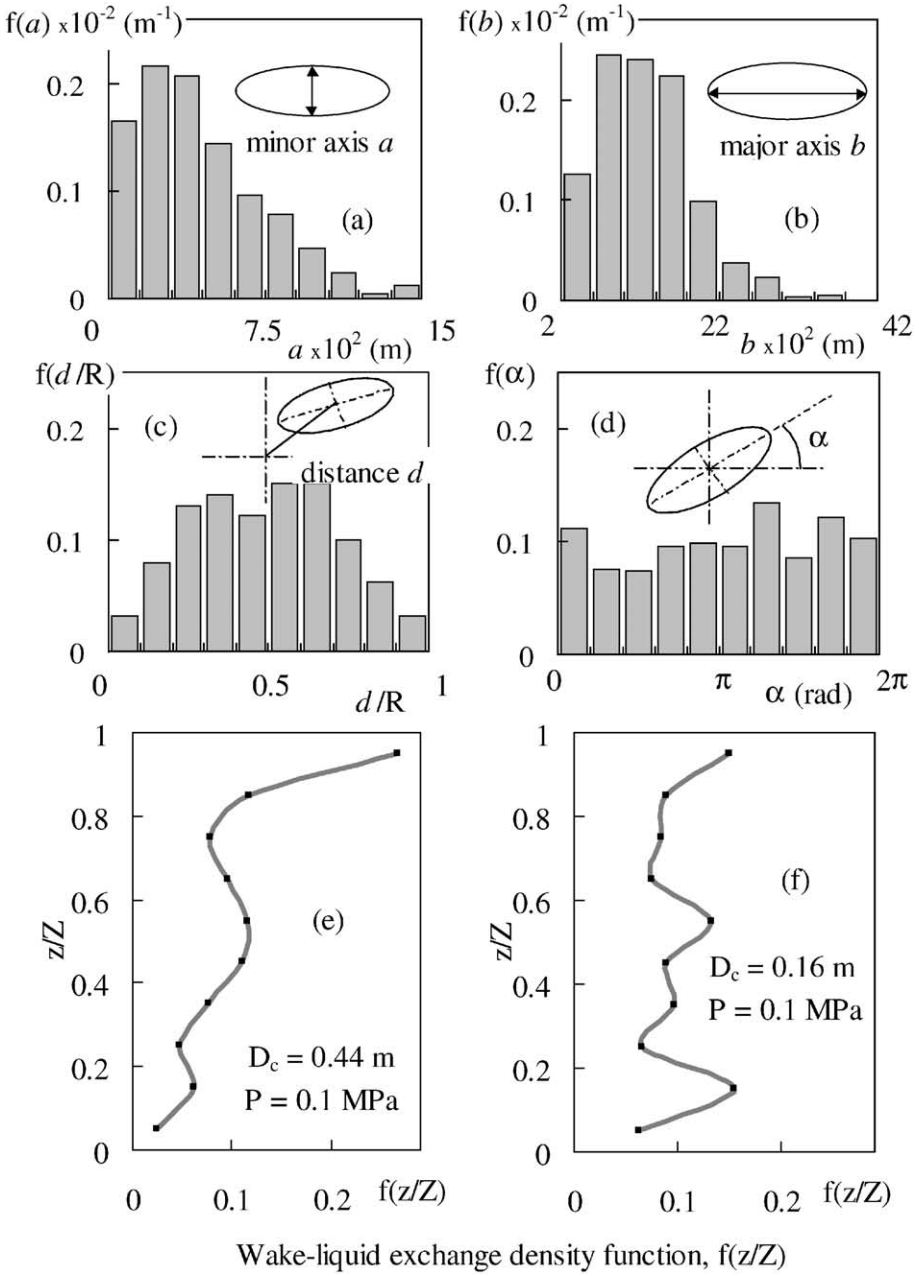

Fig. 4. Probability distributions of parameters describing the bubble-wake domain containing ellipses for the column of $D_c = 0.44$ m: (a) minor axis, (b) major axis, (c) distance between ellipse centroid and column center, (d) angle between ellipse major axis and column x-axis. Influence of the column diameter on the wake-liquid exchange axial profile for $U_G = 5$ cm/s, $P = 0.1$ MPa, (e) $D_c = 0.44$ m, (f) $D_c = 0.16$ m.

liquid dynamics. The associated eigenvectors provide a new basis for the embedding state space on which a neat image of the attractor projection can be obtained.

Projections of the reconstructed attractors from the tracer axial-coordinate time series on the first three components of the new basis of the embedding space are shown in Fig. 5 for the three runs of Table 2. The column diameter seems to affect the attractor size but not its orbits entanglement and density (Figs. 5a and b). On the contrary, increased pressure shrinks the attractor size while increasing the attractor density of orbits (Fig. 5c). Kang et al. (2000), who characterized chaos in bubble columns using pressure signal fluctuations, observed similar reconstructed attractors' patterns at increasing pressures.

Probabilistic attractor dimensions provide an indication of the number of degrees of freedom a dynamical system possesses, i.e., number of variables needed to describe the system's asymptotic state. Among them, the "correlation dimension", ν, is the easiest to compute from a time series. The Grassberger and Procaccia (1983a) algorithm

Table 3
Correlation dimension and volume-averaged Kolmogorov entropy

Gas velocity U_G (m/s)	0.04	0.04	0.05	0.05 (0.3 MPa)	0.05
Column diameter (m)	0.10	0.19	0.16	0.16	0.44
Correlation dimension	7.2	9.1	8.3	4.0	10.5
Kolmogorov entropy (bits/s)	8.6	8.8	9.7	6.2	9.6

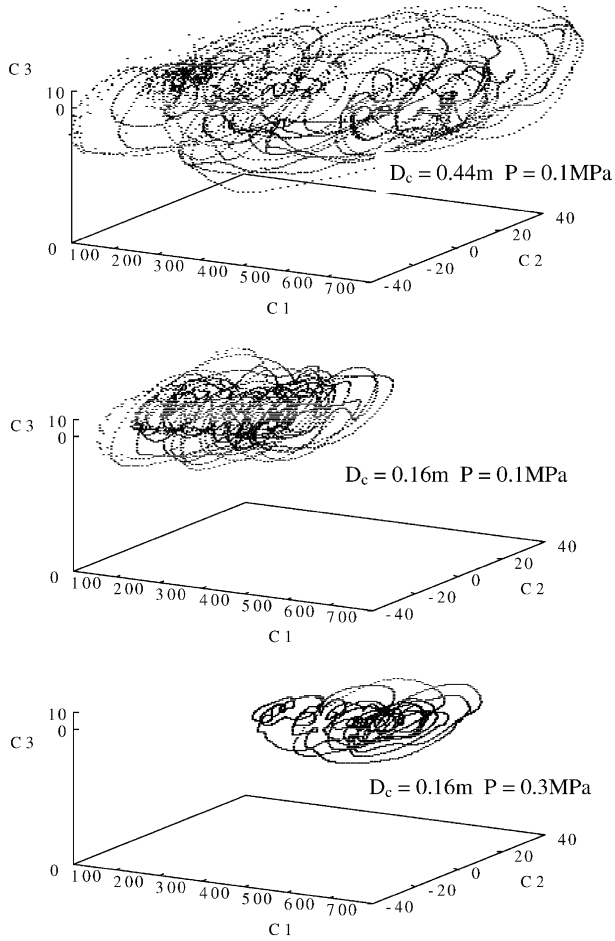

Fig. 5. Reconstructed attractors projected on the first 3 principal eigenvectors obtained by singular value decomposition for the runs of Table 2.

modified according to Theiler (1991) was used to calculate the v values listed in Table 3. The delayed time, embedding dimension and minimum number of data required to get reliable estimations were determined by trial and error, following the procedure described in Cassanello, Larachi, Marie, Guy, and Chaouki (1995). Relatively large v values are obtained for the atmospheric pressure runs. For larger column diameters, larger v values are obtained. On the other hand, the larger the pressure, the smaller is the correlation dimension. Variations in v may be associated with bubble size. Bubbles are larger in larger columns and smaller at higher pressure (Wilkinson & van Dierendonck, 1990). Kang et al. (2000) also observed a decrease in the calculated v values for higher pressures.

3.2.2. *Information loss rate—overall index*

An important feature of a chaotic system is its information loss rate (ILR), i.e., the required accuracy in the initial conditions to achieve prediction of the system evolution over a given time interval (Ott, 1993). In chaotic systems, information loss arises from exponential divergence of close trajectories in the phase space as time elapses. The Kolmogorov entropy (KE) provides quantification of the ILR. For non-chaotic systems, $KE = 0$. For a random process, $KE = \infty$, making impossible the system state assessment even after a differential time step. Chaotic systems have finite and positive KEs (Ott, 1993). For design and scale-up of fluidized beds, KE has been shown to be an appropriate invariant to characterize reactor dynamics (Schouten, Zijerveld, & van den Bleek, 1999; Schouten, van der Stappen, & van den Bleek, 1996). It is thus worthwhile to study KE variations in bubble columns.

Lower-limit estimates of KE from the tracer z coordinate time series are obtained by the algorithm of Grassberger and Procaccia (1983b). Calculated KEs (listed in Table 3) are positive, indicating that the liquid motion is chaotic. KEs compare well with those reported for bubble columns by Letzel et al. (1997), Ruzicka, Drahos, Zahradnik, and Thomas (1997) and Ruzicka, Drahos, Zahradnik, and Thomas (2000) and by Cassanello et al. (1995) for light solids in three-phase fluidization. Contrary to v, KE is barely affected by column diameter. However, it should be kept in mind that the height and aspect ratios of the analyzed experiments are different. This may prevent rigorous comparison based on KEs since high liquid height promotes bubble lateral interactions (Ruzicka et al., 2000) that may influence the information loss rate.

When increasing pressure, KE drops sharply due to a shift of the dispersed-to-coalesced transition to higher gas velocities (Wilkinson & van Dierendonck, 1990; Reilly, Scott, De Brujin, & McIntyre, 1994). KE was shown to reach minimum values at the transition between the dispersed and coalesced flow regimes (Letzel et al., 1997; Ruzicka et al., 2000).

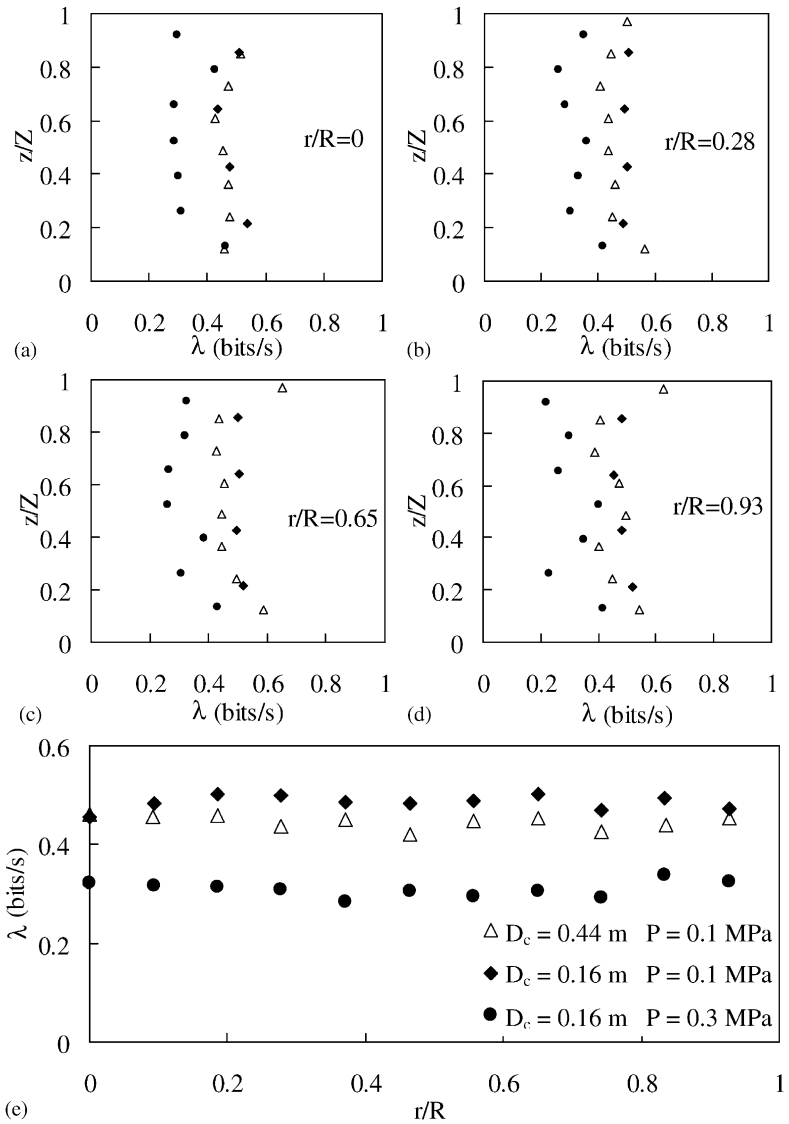

Fig. 6. Axial (a–d) and radial (e) profiles of the information loss rate quantifiers. Axial profiles obtained by average of eight azimuthal positions; mean uncertainty for each estimator around 8%. Radial profiles obtained by longitudinal averaging of the local quantifiers in the flow-developed region.

3.2.3. Information loss rate—local index

KEs as determined above are global chaos indexes. From CARPT experiments, it is also possible to estimate a local index providing insight into the divergence rate of close trajectories of fluid elements. For this purpose, the tracer trajectory is analyzed in the (x, v_x, y, v_y, z, v_z) state space, to compute a mean divergence rate, λ, of trajectories starting at very close points as

$$\lambda = \frac{1}{N_T} \sum_{n=1}^{N_T} \frac{1}{n} \log_2 \left(\frac{d_n}{d_0} \right), \tag{1}$$

where N_T is the number of pairs of close trajectories, d_0 and d_n are the distances in the state space between such pairs of trajectories at $t = 0$ and after "n" sample periods. In this way, local Lyapunov exponents (Hilborn, 1994) for different locations in the bubble column can be calculated. Since the liquid motion is bounded by the column extremes, the value of λ was computed from the slope in a plot of the mean logarithmic divergence vs. "n" before any of the trajectories reach the boundaries. The mean relative uncertainty in the estimated values, calculated as the mean of fitted slopes standard deviations, is around 8%. It depends slightly on location due to the different number of trajectories found.

Longitudinal profiles of λ at four radial locations are shown in Figs. 6a–d for the three runs of Table 2. Each datum in the figure is an average of values calculated at eight azimuthal positions. There is an almost uniform axial distribution of the ILR except near the column top and bottom limits, where λ tends to increase.

Taking into account the Lyapunov exponents only in the fully developed region, radial distributions of λ have been determined by azimuthal and longitudinal averaging (Fig. 6e). Virtually, no radial dependence for the three runs tested was found. There is a slight increase in ILR in the smaller vessel, but a marked decrease in λ as the pressure is increased. Similar axial/radial profiles have been reported for local KE determined in gas circulating fluidized beds by Ji, Ohara, Kuramoto, Tsutsumi, Yoshida, and Hirama (2000) from time series of three variables, namely pressure fluctuations, local bed voidage and heat transfer rate.

4. Conclusion

The liquid dynamics studied by CARPT was examined by applying Lagrangian (LT) and qualitative dynamics tools (QDT) in bubble columns of different sizes at different pressures. The following conclusions can be drawn:

- LT identifies the influence of pressure and column diameter on the tracer Lagrangian trajectory.
- LT reflects the behavior of the wake-generating bubbles from the tracer fast ascending journeys. Faster or larger bubbles occur in larger columns and at lower pressures.
- The liquid motion is chaotic as revealed by QDT, since the Kolmogorov entropy is positive.
- The information loss rate strongly depends on pressure but is weakly sensitive to vessel diameter.

Notation

a, b, d, α	parameters of the wake-domain-region containing ellipses, m, m, m, rad
C	vector of the new basis of the state space obtained by singular value decomposition, dimensionless
P	pressure, Pa
r	tracer radial coordinate, m
R	column radius, m
t	time, s
u_{lb}, u_{sb}	large and small bubbles velocity, m/s
U_G	superficial gas velocity, m/s
v_x, v_y, v_z	tracer velocity components, m/s
x, y, z	tracer Cartesian coordinates, m
Z	liquid height, m

Greek letter

λ	local quantifier for the information loss rate, bits/s

Acknowledgements

M.C. acknowledges financial support from Universidad de Buenos Aires and CONICET (Argentina). The co-authors from CREL at Washington University (A.K., M.A., M.P.D.) are grateful to the US Department of Energy (DE FG 1C 95212 and DE FC PC 95051) that made CARPT studies of bubble columns possible.

References

Broomhead, D. S., & King, G. P. (1986). Extracting qualitative dynamics from experimental data. *Physica D*, *20*, 217–236.

Brucker, C. (1999). Structure and dynamics of the wake of bubbles and its relevance for bubble interaction. *Physics of Fluids*, *11*, 1781–1796.

Cassanello, M., Larachi, F., Marie, M., Guy, C., & Chaouki, J. (1995). Experimental characterization of the solid phase chaotic dynamics in three-phase fluidization. *Industrial and Engineering Chemistry Research*, *34*, 2971–2980.

Chaouki, J., Larachi, F., & Dudukovic, M. P. (Eds.) (1997). *Non-invasive monitoring of multiphase flows*. Amsterdam, The Netherlands: Elsevier.

Chen, J., Kemoun, A., Al-Dahhan, M. H., Dudukovic, M. P., Lee, D. J., & Fan, L.-S. (1999). Comparative hydrodynamic study in a bubble column using computer-automated radioactive particle tracking CARPT/computed tomography and particle image velocimetry (PIV). *Chemical Engineering Science*, *54*, 2199–2207.

Chen, R. C., Reese, J., & Fan, L. S. (1994). Flow structure in a three dimensional bubble column and three-phase fluidized bed. *A.I.Ch.E. Journal*, *40*, 1093.

Deckwer, W.-D., & Schumpe, A. (1993). Improved tools for bubble column reactor design and scale-up. *Chemical Engineering Science*, *48*, 889–911.

Degaleesan, S. 1997. *Fluid dynamic measurements and modeling liquid mixing in bubble columns*. Ph.D. thesis, Washington University, St. Louis, USA.

Grassberger, P., & Procaccia, I. (1983a). Measuring strangeness of strange attractors. *Physica D*, *9*, 189–208.

Grassberger, P., & Procaccia, I. (1983b). Estimation of the Kolmogorov entropy from a chaotic signal. *Physical Review A*, *28*, 2591–2593.

Hilborn, R. C. (1994). *Chaos and nonlinear dynamics. An introduction for scientists and engineers*. New York: Oxford University Press.

Ji, H., Ohara, H., Kuramoto, K., Tsutsumi, A., Yoshida, K., & Hirama, T. (2000). Nonlinear dynamics of gas–solid circulating fluidized-bed system. *Chemical Engineering Science*, *55*, 403–410.

Kang, Y., Cho, Y. J., Woo, K. J., Kim, K. I., & Kim, S. D. (2000). Bubble properties and pressure fluctuations in pressurized bubble columns. *Chemical Engineering Science*, *55*, 411–419.

Larachi, F., Cassanello, M. C., Chaouki, J., & Guy, C. (1996). Flow structure of the solids in a 3-D gas–liquid–solid fluidized bed. *A.I.Ch.E. Journal*, *42*, 2439–2452.

Letzel, H. M., Schouten, J. C., Krishna, R., & van den Bleek, C. M. (1997). Characterization of regimes and regime transitions in bubble columns by chaos analysis of pressure signals. *Chemical Engineering Science*, *52*, 4447–4459.

Mittoni, L. J., Schwarz, M. P., & La Nauze, R. D. (1995). Deterministic chaos in the gas inlet pressure of gas–liquid bubbling systems. *Physics of Fluids*, *7*, 891–893.

Ott, E. (1993). *Chaos in dynamical systems*. New York: Cambridge University Press.

Ranade, V. V., & Utikar, R. P. (1999). Dynamics of gas–liquid flows in bubble column reactors. *Chemical Engineering Science*, *54*, 5237–5243.

Reilly, I., Scott, D., De Brujin, T., & McIntyre, D. (1994). The role of gas momentum in determining gas holdup and hydrodynamic flow regimes in bubble columns. *Canadian Journal of Chemical Engineering*, *72*, 3–12.

Ruzicka, M. C., Drahos, J., Zahradnik, J., & Thomas, N. H. (1997). Intermittent transition from bubbling to jetting regime in gas–liquid two phase flows. *International Journal of Multiphase Flow*, *23*, 671–682.

Ruzicka, M., Drahos, J., Zahradnik, J., & Thomas, N. H. (2000). Structure of gas pressure signal at two-orifice bubbling from a common plenum. *Chemical Engineering Science*, *55*, 421–429.

Schouten, J. C., van der Stappen, M. L., & van den Bleek, C. M. (1996). Scale-up of chaotic fluidized bed hydrodynamics. *Chemical Engineering Science*, *51*, 1991–2000.

Schouten, J. C., Zijerveld, R. C., & van den Bleek, C. M. (1999). Scale-up of bottom-bed dynamics and axial solids-distribution in circulating fluidized beds of Geldart-B particles. *Chemical Engineering Science*, *54*, 2103–2112.

Takens, F. (1981). *Lecture notes in mathematics*. Vol. 898 (p. 366). New York: Springer.

Theiler, J. (1991). Comments on the correlation dimension of $1/f^{\alpha}$ noise. *Physics Letters A*, *155*, 480–493.

Tritton, D. J., & Egdell, C. (1993). Chaotic bubbling. *Physics of Fluids A*, *5*, 503–505.

Tufaile, A., & Sartorelli, J. (2000). Chaotic behavior in bubble formation dynamics. *Physica A*, *275*, 336–346.

Wilkinson, P. M., & van Dierendonck, L. L. (1990). Pressure and gas density effects on bubble break up and gas hold-up in bubble columns. *Chemical Engineering Science*, *45*, 2309–2315.

Wilkinson, P. M., Spek, A. P., & van Dierendonck, L. L. (1992). Design parameters estimations for scale-up of high pressure bubble columns. *A.I.Ch.E. Journal*, *38*, 544–554.